Black: referee's comments red: authors' answers
First of all, we want to thank the two referees for the detailed analysis of our paper.
For the details, please look into the paper with keeping track of changes.

Referee #1

General comments: This manuscript presents a generally well written study on ozone retrievals from ground-based Fourier-transform infrared (FTIR) solar absorption spectra in the 3040 cm-1 spectral region. This is not a new approach, it was previously used (Rinsland et al., 1996; Goldman et al., 1999; Meier et al., 2005; Fu et al., 2007; Sung et al., 2007) for ozone retrievals, and as the study shows, this is not an optimal region for retrieving ozone. The 1000 cm-1 region proved to be more adequate for this purpose (Lindenmaier et al., 2010), and was adopted by the Network for the Detection of Atmospheric Composition Change for its harmonized FTIR ozone retrieval strategy (Vigouroux et al., 2015). However, for this particular site, Xianghe, where the spectral range is limited to the 1800 - 11000 cm-1 domain, it can give useful information about the seasonal ozone variations and its long-term trends. This retrieval approach can be extended to other FTIR sites recording spectra in this range. Therefore, I recommend this study for publication in AMT after minor revisions.

1) P3L25 – You mention "One specific optical bandpass filter. . .." Can you please be more specific? Is that the standard narrow bandpass Filter 3 (2420-3080 cm-1) used by the NDACC-IRWG community? Is it wedged?
Yes. The filter used in Xianghe is the standard narrow bandpass Filter 3 (2420-3080 cm^{-1}) used by the NDACC-IRWG community, and it is wedged. This information is added in the paper.

2) P4L2 – Explain what is epsilon.
Done

3) P4L12-14 – What was the criteria for choosing these three particular windows for your retrievals? In the 2000 – 4000 cm-1 there are other windows that could be used for ozone retrievals, e.g. 2775 cm-1, 3023 cm-1. Also, you affirm that the first window has the strongest ozone absorption lines and the least interference with H2O. Why did you add the other two? Wouldn't have been enough to use only the first? You should explain in the text. Also, clarify if these windows were used simultaneously.
Thanks for the comments/suggestions. More texts are added in the revised version.

Comparing to 2775 cm^{-1}, the O_3 lines around 3040 cm^{-1} have stronger intensity. Comparing to 3023 cm^{-1}, the O_3 lines around 3040 cm^{-1} have less impact from other species, especially from H_2O. The retrieval windows used in this study are basically from Garcia's choise with some modification. We replace one of their windows with the window 1 in this study, which has less H_2O influence. The comparison between the retrieved O_3 total column using Garcia's windows and our windows is added in the revised paper: it is found that the retrieved O_3 total columns from Garica's windows and our choices are very close to each other. However, we have more successful retrievals when using the windows in this study compared to the one using Garcia's window.

The 3 retrieval windows are used simultaneously. Using three window together allows us to get a larger DOFS (2.4) compared to only using first window (1.5). According to Figure 1, the first window has the strongest ozone absorption lines and the least interference with H_2O, but the latter two windows have more weak absorptions, which have more information in the stratosphere.

4) P4L19-20 – Have you tried fitting the minor interfering species to improve the residual? For example, for the 3039.9 – 3040.6 cm-1 window, what is the result if you fit also CH3Cl? Solar lines are not mentioned at all in the text, only in the caption of Figure 1. Among the weak species for this same window, beside solar lines you have HDO, NH3, and OH. Have you tried fitting these species? It would be great to add some text here and explain how you picked the interfering species for each window rather than just list them.
Thanks for the suggestions. Solar lines are now added in the text.
We have tested fitting the minor interfering species to improve the residual, for example adding CH_3Cl/HDO/NH_3 and OH in the window 1, the largest improvement of the RMS is less than 0.001% and the change of the retrieved O_3 total column is within 0.01%. Considering the relatively large systematic and random uncertainties of the O_3 retrieved column of 13.7/1.4%, these weak species can be ignored.

5) P5 Figure 1 – Please enlarge the panels for each window (make them as those in Figure 2 for clarity. Also, the values on the x and y axes are too small, hard to read. Bring them at the size in Figure 2.
Done

6) P9L15-20 – This part is confusing. What is the accuracy and precision of the IAP ozonsondes? What does "higher ozone detecting performance" mean? I would give numbers here, the error for the IAP ozonsondes.
Thanks for the comments. Numbers are added in the revised version. The precision of the IAP ozonsondes is within ±5% in the troposphere and within ±10% in the stratosphere, respectively.

7) P10 Figure 4 – Please enlarge the numbers on the x and y axes
Done

8) P11L6 – FTIR measurements are compared with TROPOMI OFFL at both sites, but for what window? Specify.
Added

9) P16L8 – To me it looks like it is more 10 to 40 km rather than 5 and 40 km (text). In my opinion it is not correct then to use surface to 20 km. Use 10 to 20 km in the entire manuscript, I think it is more appropriate.
Done. We change '5 and 40 km' to '10 to 40 km'.
We prefer to keep the partial column between the surface and 20 km. As the DOFS for the partial column between surface and 20km is about 1.1 (see Fig. 2), including 0.25 from surface to 10 km and 0.85 from 10 to 20 km. To have >1.0 DOFS, it is better to use the partial column between surface and 20 km. We agree with the referee that the O_3 retrieval (3040 cm^{-1}) is mainly sensitive to 10-40 km, and we highlight in the paper that the lower partial column (surface-20 km) is mainly sensitive to the upper troposphere and lower stratosphere (UTLS), and less sensitive to the boundary layer.

There are some typos in the text:
P2L15 – Change "the continue" to "to continue"
P6L24 – Change "mainly the" to "mainly from the"

P13 Figure 6 caption L5 – Change “and the back solid line” to “and the black solid line”
Corrected

References:

Rinsland CP, Connor BJ, Jones NB, Boyd I, Matthews WA, Goldman, A, et al. Comparison of infrared and Dobson total ozone columns measured from Lauder, New Zealand. Geophys Res Lett 1996; 23:1025–8.

Goldman A, Paton-Walsh C, Bell W, Toon GC, Blavier JF, Sen, B, et al. Network for the Detection of Stratospheric Change Fourier trans- form infrared intercomparison at Table Mountain Facility, Novem- ber 1996. J Geophys Res 1999; 104:30481–503.

Meier A, Paton-Walsh C, Bell W, Blumenstock T, Hase F, Goldman, A, et al. Evidence of reduced measurement uncertainties from an FTIR instrument intercomparison at Kiruna, Sweden. JQSRT 2005; 96:75–84.

Fu D, Walker KA, Sung K, Boone CD, Soucy MA, Bernath PF. The portable atmospheric research interferometric spectrometer for the infrared, PARIS-IR. JQSRT 2007; 103:362–70.

Sung K, Skelton R, Walker KA, Boone CD, Fu D, Bernath P. N2O and O3 Arctic column amounts from PARIS-IR observations: retrievals, characterization and error analysis. JQSRT 2007; 107:385–406.

Lindenmaier R, Batchelor RL, Strong K, Fast H, Goutail F, Kolonjari F, et al. An evaluation of infrared microwindows for ozone retrievals using the Eureka Bruker 125HR Fourier transform spectrometer, JQSRT 2010; 111(4):569-585.

Black: referee's comments red: authors' answers
First of all, we want to thank the two referees for the detailed analysis of our paper.
For the details, please look into the paper with keeping track of changes.

Referee #2

General comments: The authors present a study on ozone retrievals from infrared spectra recorded in Xinghe, China and on Reunion Island. Data from these sites are highly needed since these areas are poorly represented in the networks. This study uses the 3040 cm-1 spectral region and presents results of a one year time series and a characterisation of the 3040 cm-1 ozone product. Moreover, using spectra from Reunion Island data obtained from the 3040 cm-1 region are compared with those with the standard NDACC retrieval at 1000 cm-1. The comparison shows a good correlation, but a bias of 5.5 to 9.0 % and reduced degrees of freedom compared to the standard microwindow. Ozone retrievals in the 3040 cm-1 region are very useful since there are several FTIR spectrometers without an MCT detector around the globe.

For the 3040 cm-1 retrieval a modified version of the recipe of Garcia et al., 2014, was used. As a result, the key findings are very similar to those obtained by Garcia et al., 2014. However, since the recent study doesn't use exactly the same recipe, strictly speaking, it cannot be used as confirmation of the Garcia recipe and as an extension including more sites covering different conditions. To my impression, it is not clear whether it is a confirmation of the Garcia paper showing similar retrieval results or whether there is an improvement as compared to the Garcia paper. If the authors claim the latter this should be demonstrated or at least discussed in detail. To do so the authors might think in adding a Garcia type retrieval for comparison.

Therefore, I would recommend publishing this paper after major revisions although the paper is well written and fits well to the scope of AMT. Please also see specific comments below.

Specific comments:

- The statement in the abstract 'as the harmonized . . . uses the 1000 cm-1 spectral range, we designed an alternative O3 retrieval strategy . . .' is not correct since there is a published 'alternative' retrieval recipe for FTIR sites without MCT detector as published by Garcia et al., 2014.

Thanks for pointing out the inappropriate statement.
The sentence is reworded in the revised version "we apply the O3 retrieval in the 3040 cm−1 spectral range at Xianghe."

- The recipe from Garcia et al. 2014, has been modified. The modifications made and the rationale behind these modifications should be described in more detail. Moreover, a comparison with retrieval results using the full recipe from Garcia et al. would be very useful to see the effect of these modifications.

Thanks for the suggestion. The comparison between the FTIR O_3 retrievals using the window in this study and García et al., 2014 window has been added in the Appendix A of the revised paper.

In general, the retrieved O_3 total columns at Xianghe using the windows in this study and the window from García et al. 2014 are very close to each other. The mean and standard deviation of their relative difference are 0.8% and 1.2%, which are quite small compared to the retrieval uncertainty. However, we have more successful retrievals when using the windows in this study compared to their window choice, especially in summer with more H2O. The RMS of the residual using the windows in this study is about 0.20%, which is less compared to the one using Garcia's window of about 0.24% mainly due to several bad CH_4 fittings. In addition, the mean of daily standard deviation of the retrieved total column for all days with more than 4 measurements using the García's window is 1.4%, which is slightly larger compared to 1.3% using the windows in this study. As the water vapor abundance is relatively high in summer at Xianghe, we suggest using the window of 3039.9-3040.6 cm^{-1} instead of the window of 3042.48-3043.72 cm^{-1}.

- p. 4: 'a few badly fitted absorptions': Fig. 1 shows strong residuals at ozone line positions in particular in microwindow 1, not included in the Garcia paper. Does this additional window really improves the fit results although the line list needs improvement for this window?
Thanks for the comments. By comparing FTIR O_3 [3040 cm^{-1}] retrievals with other datasets (FTIR O_3 [1000 cm^{-1}] retrievals, FTIR O_3 [3040 cm^{-1}] retrievals using García's window and TROPOMI measurements), it is found that the FTIR O_3 [3040 cm^{-1}] retrievals are generally in good agreement with other datasets apart from a systematic uncertainty. Adding the microwindow 1 does not harm the retrieval, although the O_3 lines are not perfectly fitted. On the contrary, by adding the microwindow 1, the O_3 retrieval has more information in the troposphere due to a stronger O_3 line intensity compared to the lines in microwindows 2 and 3. The averaged DOF is 2.2 using only bands 2 and 3, and the DOF is 2.4 using 3 bands together at Xianghe.

- p. 3: 'One specific optical bandpass filter (2000 – 4000 cm-1)': This is not the standard NDACC type optical filter. The NDACC type filters provide a smaller bandwidth and increase the signal to noise ratio.
The filter used in Xianghe is the standard narrow bandpass Filter 3 (2420-3080 cm^{-1}) used by the NDACC-IRWG community, and it is wedged. This information is added in the paper.

- p. 4: 'the ILS . . . retrieved simultaneously . . .': Since differences to the ideal ILS are hardly to distinguish with differences of the profile shape it is strongly recommended to retrieve the ILS from cell spectra. How does the resulting ILS looks like? Does it differ with respect to the ideal ILS and how much does it vary with time?
Thanks for the comments.
Simultaneous retrieving ILS allows us more freedom to fit the residual. We tune the sigma of the ILS parameter in sfit4.ctl to constrain the retrieved ILS and to make it close to the ILS results derived from the LINEFIT using the HBr cell measurements. Figure 1a shows the modulation efficiencies (ME) retrieved by the LINEFIT14.5 code from 4 HBr cell measurements at Xianghe. Figure 2 shows an example of the a priori and retrieved ME, as well as the time series of the retrieved ME at the maximum optical path difference (MOPD = 175 cm). The a priori ME is the ideal status, and the retrieved ME is close to the LINEFIT results. The mean and standard deviation of the retrieved ME at the MOPD are 0.88 and 0.04, respectively, and the retrieved ME is relatively stable with time.

The LINEFIT retrieval also suffers from the uncertainties of the cell pressure, temperature and gas abundance, and it is not easy to estimate these uncertainties. Therefore, we prefer to retrieve the ILS but with a reasonable sigma to constraint the retrieved ILS parameters and to make them close to the cell measurements instead of using the LINEFIT outputs directly.

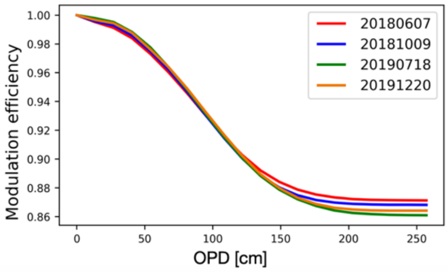

Figure 1a. The modulation efficiencies retrieved by the LINEFIT14.5 code from HBr cell measurements at Xianghe on 7 June 2018, 9 October 2018, 18 July 2019 and 20 December 2019.

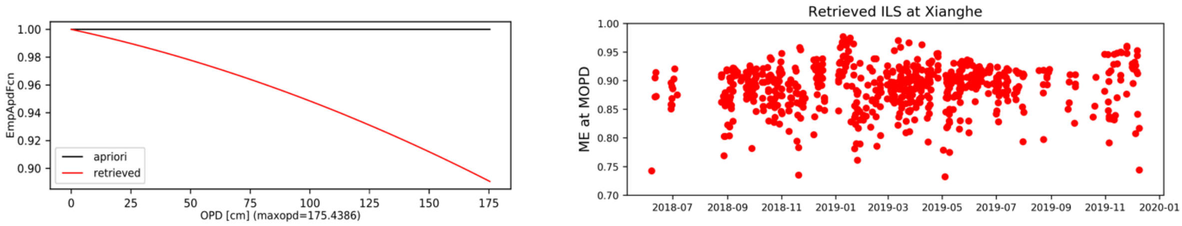

Figure 2a. Left panel: a typical example of the a priori and retrieved modulation efficiencies (ME) along with the optical path difference (OPD) at Xianghe. Right panel: the time series of the retrieved ME at the Maximum OPD (175 cm).

Technical corrections:
- p. 3, line 1: in June at Xianghe => at Xianghe in June
- p. 4, line 15: O3 retrieved profiles => retrieved O3 profiles
- p. 6, line 23: mainly the => mainly from the
– p. 7, line 4: larger the => larger as compared to the
– p. 16, line 2: a MCT => an MCT?

Corrected

Reference:

García, O. E., Schneider, M., Hase, F., Blumenstock, T., Sepúlveda, E., and González, Y.: Quality assessment of ozone total column amounts as monitored by ground-based solar absorption spectrometry in the near infrared (> 3000 cm-1), Atmos. Meas. Tech., 7, 3071–3084, https://doi.org/10.5194/amt-7-3071-2014, 2014.

Ground-based FTIR O_3 retrievals from the 3040 cm^{-1} spectral range at Xianghe, China

Minqiang Zhou[1], Pucai Wang[2,3,4], Bavo Langerock[1], Corinne Vigouroux[1], Christian Hermans[1], Nicolas Kumps[1], Ting Wang[2], Yang Yang[2], Denghui Ji[2], Liang Ran[2], Jinqiang Zhang[2], Yuejian Xuan[2], Hongbin Chen[2,3,4], Françoise Posny[5], Valentin Duflot[5,6], Jean-Marc Metzger[6], and Martine De Mazière[1]

[1]Royal Belgian Institute for Space Aeronomy (BIRA-IASB), Brussels, Belgium
[2]Key Laboratory of Middle Atmosphere and Global Environment Observation, Institute of Atmospheric Physics, Chinese Academy of Sciences, Beijing, China
[3]University of Chinese Academy of Sciences, Beijing, China
[4]Xianghe Observatory of Whole Atmosphere, Institute of Atmospheric Physics, Chinese Academy of Sciences, Xianghe, China
[5]LACy, Laboratoire de l'Atmosphère et des Cyclones, UMR8105 (CNRS, Université de La Réunion, Météo-France), Saint-Denis, Réunion, France
[6]UMS 3365 – OSU Réunion, Université de La Réunion, Saint-Denis, Réunion, France

Correspondence: Minqiang Zhou (minqiang.zhou@aeronomie.be), Pucai Wang (pcwang@mail.iap.ac.cn)

Abstract. In this study, we present O_3 retrievals from ground-based Fourier-transform infrared (FTIR) solar absorption measurements between June 2018 and December 2019 at Xianghe, China (39.75 °N, 116.96 °E). The FTIR spectrometer at Xianghe is operated with indium gallium arsenide (InGaAs) and indium antimonide (InSb) detectors, recording the spectra between 1800 and 11000 cm^{-1}. As the harmonized FTIR O_3 retrieval strategy (Vigouroux et al., 2015) within the Network for the Detection of Atmospheric Composition Change (NDACC) uses the 1000 cm^{-1} spectral range, we ~~designed an alternative~~ apply the O_3 retrieval ~~strategy~~ in the 3040 cm^{-1} spectral range at Xianghe.

The retrieved O_3 profile is mainly sensitive to the vertical range between ~~5~~ 10 and 40 km, and the degree of freedom for signal is 2.4±0.3 (1σ), indicating that there are two individual pieces of information in partial columns between the surface and 20 km and between 20 and 40 km. According to the optimal estimation method, the systematic and random uncertainties of the FTIR O_3 total columns are about 13.6% and 1.4%, respectively. The random uncertainty is consistent with the observed daily standard deviation of the FTIR retrievals.

To validate the FTIR O_3 total and partial columns, we apply the same O_3 retrieval strategy at Maïdo, Reunion Island (21.08 °N, 55.38 °E). The FTIR O_3 (3040 cm^{-1}) measurements at Xianghe and Maïdo are then compared with the nearby ozonesondes at Beijing (39.81 °N, 116.47 °E) and at Gillot (20.89 °S, 55.53 °E), respectively, as well as with co-located TROPOspheric Monitoring Instrument (TROPOMI) satellite measurements at both sites. In addition at Maïdo, we compare the FTIR O_3 (3040 cm^{-1}) retrievals with the standard NDACC FTIR O_3 measurements using the 1000 cm^{-1} spectral range. It is found that the total columns retrieved from the FTIR O_3 3040 cm^{-1} measurements are underestimated by 5.5 - 9.0 %, which is mainly due to the systematic uncertainty in the partial column between 20 and 40 km (about -10.4%). The systematic uncertainty in the partial column between surface and 20 km is relatively small (within 2.4%). By comparison with other

measurements, it is found that the FTIR O_3 (3040 cm^{-1}) retrievals capture very well the seasonal and synoptic variations of the O_3 total and two partial columns. Therefore, the ongoing FTIR measurements at Xianghe can provide useful information on the O_3 variations and (in the future) long-term trends.

1 Introduction

Ozone (O_3) is an important atmospheric trace species: about 90% of the O_3 abundance is in the stratosphere, where it protects life on the Earth's surface from harmful ultraviolet (UV) rays from the sun in the stratosphere (IPCC, 2013). The main source of stratospheric O_3 is a photochemical process involving oxygen, the so-called Chapman cycle (Langematz, 2019). The stratospheric O_3 was observed to decrease since the 1970s, and it was found that this depletion is highly related to the release of chlorofluorocarbons and other halocarbons by mankind (Molina and Rowland, 1974; Montzka et al., 1996). Therefore, 27 nations around the world signed the Montreal Protocol in 1987 to control the emissions of the ozone-depleting species (Murdoch and Sandler, 1997). However, Montzka et al. (2018) monitored an unexpected and persistent increase in global emissions of trichlorofluoromethane (CFC-11) since 2017, and Rigby et al. (2019) pointed out that the increase in CFC-11 emission is attributed to eastern China. Lickley et al. (2020) recently found that CFC-11 and dichlorodifluoromethane (CFC-12) leaking out of old cooling equipment and from building insulation are much larger than had been estimated. Therefore, it is very important ~~the~~ to continue the monitoring of ozone all over the world. The remaining ~10% amount of O_3 is located in the troposphere, where it is a pollutant gas that is produced, among others, from interactions with nitrogen oxides and volatile organic compounds (Monks et al., 2015). In addition, the O_3 in the free troposphere is also an important greenhouse gas (IPCC, 2013). Xianghe (39.75 °N, 116.96 °E, 50 m a.s.l.), a site located about 50 km east to Beijing, is in a polluted region in North China, with large anthropogenic emissions for O_3 precursor gases: carbon monoxide, nitrogen oxides, non-methane volatile organic compounds and methane (European Commission, 2013). Previous studies found that the tropospheric O_3 concentrations around Beijing increase significantly since 2002 (Wang et al., 2012; Zhang et al., 2014a; Ma et al., 2016). The high tropospheric O_3 concentration has become a serious air pollutant in China, and the tropospheric O_3 level in 2015 led to a noticeable increased premature mortality of 0.9% (Feng et al., 2019).

The ground-based Fourier-transform infrared (FTIR) solar absorption spectrometry is a well-established remote sensing technique, which measures an ever-increasing list of chemical compounds along the entire line-of-sight between the ground-based instrument and the sun, thus providing information about the total column as well as the vertical profile for some species, on both short and very long time scales. Within the Network for the Detection of Atmospheric Composition Change - Infrared Working Group (NDACC-IRWG), O_3 is an important target gas (De Mazière et al., 2018), and there are about 20 active FTIR sites around the world providing ongoing O_3 measurements (http://www.ndacc.org/). The O_3 retrieval strategy has been harmonized within NDACC (Vigouroux et al., 2015) and uses the absorption around 1000 cm^{-1} from the spectra recorded with a mercury cadmium telluride (MCT) detector. As NDACC provides long-time series of O_3 measurements with high accuracy and precision, these data are used to understand the atmospheric O_3 trend (Vigouroux et al., 2015; Steinbrecht et al., 2017), and to validate the satellite measurements (Boynard et al., 2018).

A ground-based FTIR spectrometer (Bruker IFS 125HR) has been installed ~~in June 2018~~ at Xianghe (39.75°N, 116.96°E; 50 m a.s.l.) in June 2018 to measure the atmospheric carbon dioxide, methane and carbon monoxide (Yang et al., 2019). The FTIR instrument at Xianghe is operated with indium gallium arsenide (InGaAs) and indium antimonide (InSb) detectors, recording the spectra with a spectral range from 1800 to 11000 cm^{-1}. Therefore, the NDACC standard O_3 retrieval strategy cannot be applied directly to the Xianghe spectra. Several other infrared microwindows, which have been applied to retrieve O_3 from the ground-based FTIR spectra: Lindenmaier et al. (2010) summarized all the related FTIR O_3 studies, and it appears that the 3040 cm^{-1} range is often used within the ground-based FTIR community. Takele Kenea et al. (2013) used six micro-windows in the spectral range of 3039.37-3051.90 cm^{-1} for the O_3 retrieval at Addis Ababa, Ethiopia. García et al. (2014) tested O_3 retrievals in both 3040 and 4030 cm^{-1} ranges at Izaña, Spain, and they found that the precision of O_3 total column retrievals from the 3040 cm^{-1} range is 2%, which is much better than the 5% precision obtained in the 4030 cm^{-1} range. However, they found that the total column of O_3 from the 3040 cm^{-1} range is about 7% smaller than that retrieved in the standard NDACC 1000 cm^{-1} range.

The aim of this paper is to study the FTIR O_3 retrieval in the 3040 cm^{-1} spectral range at Xianghe, and to evaluate the retrieval uncertainty. Section 2 presents the retrieval strategy and the characteristics of the FTIR O_3 retrieval at Xianghe. After that, we show the time series and seasonal variations of FTIR O_3 retrievals between June 2018 and December 2019. In section 3, the same retrieval strategy is applied to Maïdo, Reunion Island (21.08 °N, 55.38 °E; 2155 m a.s.l.), which is a NDACC-IRWG affiliated instrument. At both sites, we compare the FTIR O_3 measurements with the nearby ozonesonde measurements and the co-located TROPOspheric Monitoring Instrument (TROPOMI) satellite measurements. In addition, the FTIR O_3 retrievals (3040 cm^{-1}) are compared to standard NDACC FTIR O_3 retrievals (1000 cm^{-1}) at Maïdo. Finally, the conclusions are drawn in Section 4.

2 FTIR O_3 retrievals at Xianghe

The FTIR site at Xianghe Observatory of Whole Atmosphere is operated by the Institute of Atmospheric Physics (IAP), the Chinese Academy of Sciences (CAS). The FTIR system includes a Bruker IFS 125HR instrument, an automatic weather station and a sun tracker system (Yang et al., 2019). The spectra suitable for O_3 retrievals are recorded with a maximum optical path difference of 180 cm, corresponding to a spectral resolution of 0.005 cm^{-1}. ~~One specific optical bandpass filter (2000 - 4000~~ The standard wedged narrow bandpass filter 3 (2420-3080 cm^{-1}) used by the NDACC-IRWG community is inserted in front of the InSb detector in order to improve the signal-to-noise (SNR). The mean SNR of the spectra used in this study is about 1400.

2.1 Retrieval strategy

The SFIT4_v9.4.4 algorithm (Pougatchev et al., 1995) is applied to retrieve the O_3 profile using the optimal estimation method (OEM) (Rodgers, 2000)

$$\boldsymbol{x}_r = \boldsymbol{x}_a + \mathbf{A}(\boldsymbol{x}_t - \boldsymbol{x}_a) + \boldsymbol{\epsilon}, \tag{1}$$

where $\boldsymbol{x}_r$, $\boldsymbol{x}_a$ and $\boldsymbol{x}_t$ are retrieved, a priori and true state vectors (all retrieved parameters) and $\mathbf{A}$ is the averaging kernel, representing the sensitivity of the retrieved parameters to the true status, $\boldsymbol{\epsilon}$ is the retrieved error. The SFIT4 algorithm minimizes the cost function ($\boldsymbol{J}(\boldsymbol{x})$)

$$\boldsymbol{J}(\boldsymbol{x}) = [\boldsymbol{y} - \boldsymbol{F}(\boldsymbol{x})]^T \mathbf{S}_{\boldsymbol{\epsilon}}^{-1} [\boldsymbol{y} - \boldsymbol{F}(\boldsymbol{x})] + [\boldsymbol{x} - \boldsymbol{x_a}]^T \mathbf{S}_a^{-1} [\boldsymbol{x} - \boldsymbol{x_a}], \tag{2}$$

where $\boldsymbol{y}$ and $\boldsymbol{F}(\boldsymbol{x})$ are the observed and fitted spectra, respectively, $\mathbf{S}_{\boldsymbol{\epsilon}}$ is the measurement covariance matrix and $\mathbf{S}_a$ is the a priori covariance matrix. $\boldsymbol{J}(\boldsymbol{x})$ is the combination of the measurement information and the a priori information, with their weightings determined by $\mathbf{S}_{\boldsymbol{\epsilon}}$ and $\mathbf{S}_a$. $\mathbf{S}_{\boldsymbol{\epsilon}}$ is derived from the SNR of the spectra, with its diagonal values set to $1/\mathrm{SNR}^2$ and off-diagonal values to 0. $\mathbf{S}_a$ is derived from the covariance matrix of the Whole Atmosphere Community Climate Model (WACCM) v6 O_3 monthly means between 1980 and 2020. The square root of the diagonal elements of $\mathbf{S}_a$ are about 3% near the surface, 2% in the troposphere, 2.5% in the stratosphere and 1% above the stratosphere.

Table 1 lists the parameters adopted in the retrieval strategy for the FTIR O_3 measurements at Xianghe in this study. We selected three retrieval windows (3039.9 - 3040.6 cm^{-1}, 3041.5 - 3042.25 cm^{-1} and 3044.7 - 3045.54 cm^{-1}) in this study, where the latter two windows are taken from the study of García et al. (2014); the first window has the strongest O_3 absorption lines and the least interference with H_2O. Comparing to the retrieval windows used in García et al. (2014), the FTIR O_3 retrieved total columns from the three windows in this study are similar but slightly less affected by H_2O abundances ~~, and the O_3 retrieved profiles are less oscillating by comparison with ozonesonde profiles at Xianghe and Maïdo~~(see Appendix A). For the spectroscopic data, we use the atmospheric line list ATM2019 (https://mark4sun.jpl.nasa.gov/pseudo.html; last access: 26 March 2019). Figure 1 shows an example of the absorption lines and residuals in the three retrieval windows at Xianghe. The root mean square (RMS) of the residual is about 0.2%. It contains a few badly fitted absorptions at O_3 line positions in these 3 windows, caused by uncertainties in the spectroscopy. Further investigations are needed to improve the spectroscopic parameters in this spectral range, but that is beyond the scope of this study. To reduce the influence from the interfering species, CH_4, HCl, $H_2^{18}O$, $H_2^{17}O$, H_2O, HDO and CO_2 columns are retrieved simultaneously with the O_3 profile. The specific interfering species are selected for each window (see Figure 1), because they have relatively larger absorptions compared to other weak species, e.g. CH_3Cl, NH_3 and OH. In addition, the solar intensity and wavenumber shift are retrieved simultaneously. Note that the H_2O isotopes ($H_2^{18}O$, $H_2^{17}O$ and HDO) are treated as individual species in the SFIT4 algorithm. The instrument line shape (ILS) is part of the state vector and retrieved simultaneously along with the O_3 profile, with an ideal ILS being applied as the a priori input.

The temperature, pressure and H_2O profiles are from the National Centers for Environmental Prediction (NCEP) 6-hourly re-analysis data. For the a priori profiles of O_3 and other interfering species, we use the mean of the WACCM model data between 1980 and 2020. Since the broadening effect of absorption lines is related to the pressure and temperature, we can obtain limited vertical information of O_3 by fitting the spectra. Figure 2 shows an example of the typical averaging kernel of the FTIR O_3 retrieval at Xianghe. The retrieved O_3 profile is mainly sensitive to the vertical range between ~~5~~ 10 and 40 km. The degree of freedom for signal (DOFS) is 2.4 ± 0.3 (1σ), indicating that there are two individual pieces of information:

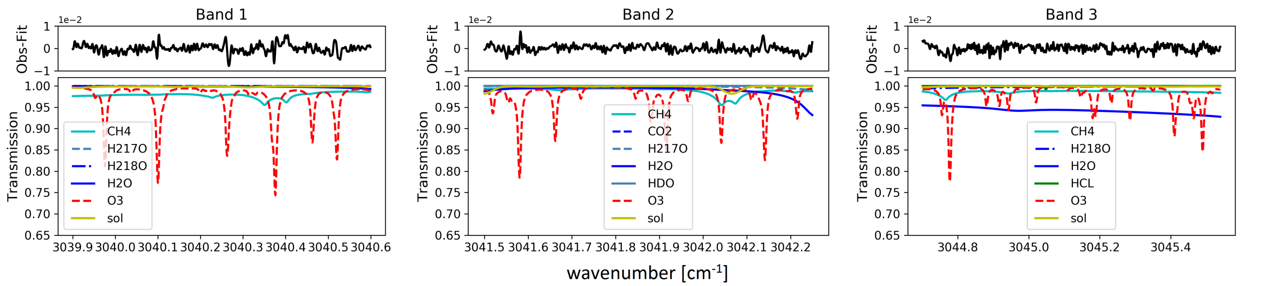

Figure 1. Example of spectral fits in the three microwindows for O_3 retrievals at Xianghe. Lower panels: the normalized transmittance from each atmospheric species and solar lines. Upper panels: the difference between the observed and fitted spectra (Obs-Fit).

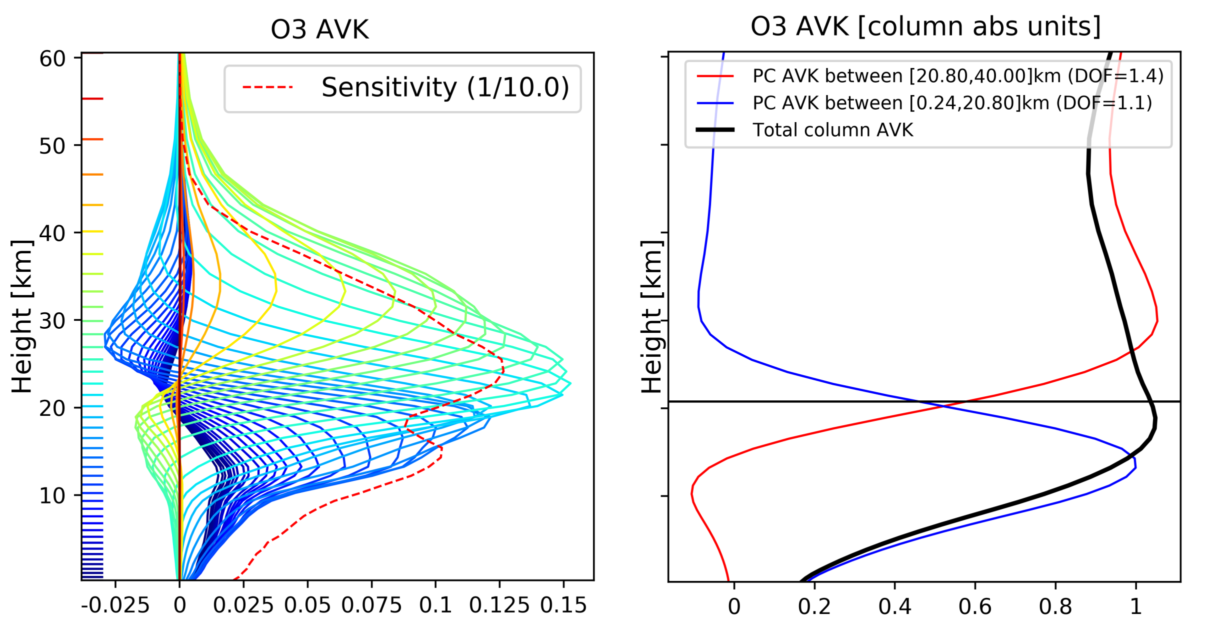

Figure 2. Typical vertical sensitivity of the O_3 retrieval at Xianghe. Left panel: the averaging kernel (AVK) matrix whose rows are color coded with the altitude of the retrieval grid (48 layers from the surface to the top of atmosphere). The red dashed line is the sensitivity curve (sum of averaging kernel rows) scaled by 1/10 to bring it to the same scale as the averaging kernel. Right panel: the total column averaging kernel (black) and the partial column (PC) averaging kernels of two individual layers (surface-20 km and 20-40 km) with DOFS equal to 1.1 and 1.4, respectively.

partial columns between the surface and 20 km, and between 20 and 40 km. Note that the lower partial column (surface-20 km) is mainly sensitive to the upper troposphere and lower stratosphere (UTLS), and less sensitive to the boundary layer.

Table 1. The retrieval strategy of the FTIR O_3 using 3040 cm^{-1} spectral range at Xianghe.

Window (cm^{-1})	3039.9 - 3040.6, 3041.5 - 3042.25 and 3044.7 - 3045.54
Profile retrieval	O_3
Column retrieval	CH_4, HCl, $H_2^{18}O$, $H_2^{17}O$, H_2O, HDO and CO_2
Spectroscopy	ATM2019
A priori profile	NCEP and WACCM
ILS	polynomial fitting with an ideal ILS as a priori input
SNR	$\sim$1400
DOFS	2.4 $\pm$ 0.3

2.2 Uncertainty estimation

According to Rodgers (2000), the error ($\boldsymbol{\epsilon}_r = \boldsymbol{x}_r - \boldsymbol{x}_t$) of the retrieved O_3 profile is

$$\boldsymbol{\epsilon_r} = (\mathbf{A} - \mathbf{I})(\boldsymbol{x_t} - \boldsymbol{x_a}) + \mathbf{G}_y\mathbf{K}_b(\boldsymbol{b_t} - \boldsymbol{b}) + \mathbf{G}_y\boldsymbol{\epsilon}_m \tag{3}$$

where $\boldsymbol{b_t}$ and $\boldsymbol{b}$ are the true and used model parameters, e. g. solar zenith angle (SZA), spectroscopy, temperature; $\mathbf{I}$ is the unit matrix; $\mathbf{G}_y$ is the contribution matrix; $\mathbf{K}_b$ is the Jacobian matrix for the model parameters; $\boldsymbol{\epsilon}_m$ is the noise of the spectra. The right side of Eq. 3 contains the smoothing error ($(\mathbf{A} - \mathbf{I})(\boldsymbol{x_t} - \boldsymbol{x_a})$), the model parameter error ($\mathbf{G}_y\mathbf{K}_b(\boldsymbol{b_t} - \boldsymbol{b})$) and the measurement noise ($\mathbf{G}_y\boldsymbol{\epsilon}_m$). For each component, the systematic and random uncertainties are estimated individually. As the state vector contains the O_3 profile, interfering species and other retrieved parameters, the smoothing error ($(\mathbf{A} - \mathbf{I})(\boldsymbol{x_t} - \boldsymbol{x_a})$) can be divided into three portions (Zhou et al., 2016), corresponding to smoothing (from the O_3 profile), interfering species and retrieval parameters in Table 2.

The $\boldsymbol{\epsilon}_m$ is derived from the SNR. The systematic uncertainties of both O_3 and interfering species a priori profiles are set to 10%, and their random uncertainties are derived from the WACCM data. According to the ATM2019 linelist, the systematic uncertainties of O_3 line intensity, air broadening and pressure broadening are 10-20%, 5-10% and 5-10%, respectively. In this study, we set 15%, 7.5% and 7.5% for the systematic uncertainties of the O_3 line intensity, air broadening and pressure broadening, respectively, and we assume that there are no random uncertainties. The uncertainties for temperature and H_2O are derived from the difference between NCEP reanalysis data and the European Centre for Medium-Range Weather Forecasts (ECMWF) ERA5 reanalysis data, where the mean difference is set as the systematic uncertainty and the standard deviation (STD) of the differences is set as the random uncertainty. The systematic uncertainty of the temperature profile is about 0.5 K for the whole altitude range, and its random uncertainty is about 2 K below 2 km and 1 K above. The random and systematic uncertainties for SZA are set to 0.5% and 0.1%, respectively. Table 2 shows the resulting total uncertainty on the retrieved O_3 total column and two partial columns. The systematic uncertainty is dominated by the uncertainty from the spectroscopy. The random uncertainty of the total column is 1.4%, which is coming mainly from the SZA and interfering species uncertainties. The random uncertainty of the lower partial column (surface-20 km) is 3.6%, which comes mainly from the smoothing error and SZA uncertainty. The random uncertainty of the upper partial column (20-40 km) is 2.2%, which comes mainly from the smoothing error and retrieval parameters uncertainties. To check the estimated random uncertainty, we calculated the mean of daily STD for all days with more than 4 measurements (see Table 2). Keep in mind that daily STD still includes the signal of the diurnal variation, therefore, it might be slightly larger as compared to the random uncertainty. In general, the STDs of the total column and the two partial columns are close to the estimated uncertainties, indicating that the random uncertainties have been estimated correctly.

Table 2. The estimated retrieval uncertainty of the retrieved O_3 total column and two partial columns at Xianghe, together with the corresponding means of the daily STD of the FTIR O_3 retrievals.

O_3	Uncertainty sources	Total column	Surface-20 km	20-40 km
Random [%]	Measurement	0.2	0.3	0.3
	Temperature	0.3	0.2	0.2
	SZA	1.0	1.0	1.0
	Retrieval parameters	0.1	0.7	1.4
	Interfering species	0.9	1.7	0.7
	Smoothing	0.6	2.9	1.2
	Total	1.4	3.6	2.2
	Daily STD [%]	1.3	3.7	1.5
Systematic [%]	Spectroscopy	13.6	11.8	16.1
	Temperature	1.4	1.7	1.9
	SZA	0.2	0.2	0.2
	Retrieval parameters	0.1	0.7	1.4
	Interfering species	0.1	0.3	0.1
	Smoothing	0.2	1.2	0.1
	Total	13.7	12.0	16.3

2.3 Time series and seasonal variations

Figure 3 shows the time series of the total column of FTIR O_3 measurements, as well as two partial columns (surface-20 km and 20-40 km) from June 2018 to December 2019 at Xianghe. The seasonal variation is fitted with a periodic third order function ($\sum_{k=1}^{3}(A_{2k-1}\cos(2k\pi \boldsymbol{t}) + A_{2k}\sin(2k\pi \boldsymbol{t})$, with t in fraction of year) using all the individual measurements. The mean total column is $8.70 \times 10^{18}\text{molecules/cm}^2$, and the mean partial columns between the surface and 20 km, and between 20 and 40 km are $3.42 \times 10^{18}\text{molecules/cm}^2$ and $5.05 \times 10^{18}\text{molecules/cm}^2$, respectively. The lower partial column (surface-20 km) has a minimum in August-September and a maximum in February-April, while the upper partial column (20-40 km) has a minimum in October-December and a maximum in May-July. The peak-to-peak amplitude of the seasonal variation in the

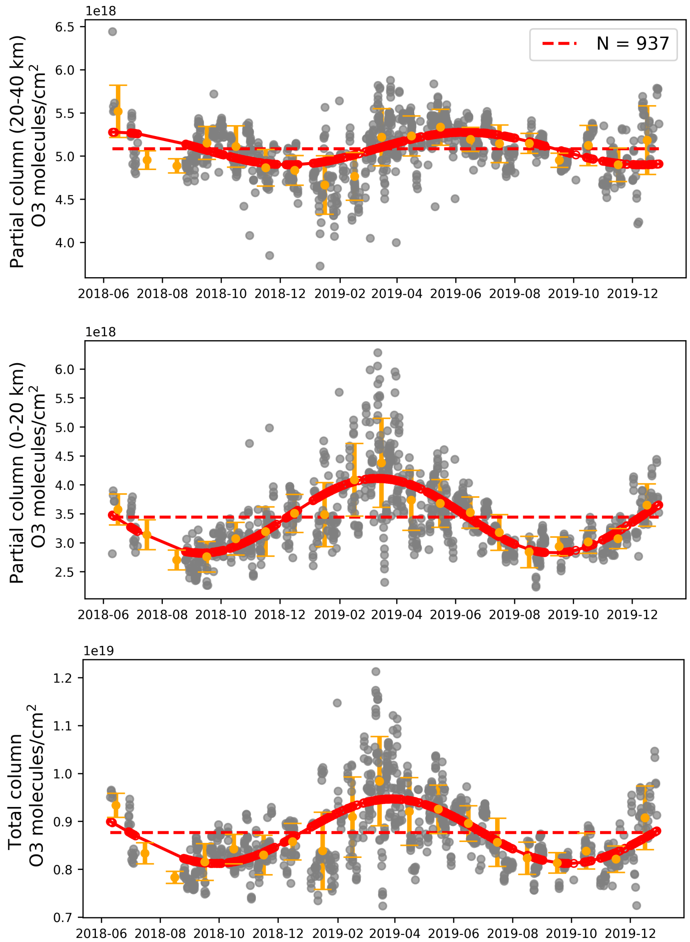

Figure 3. The time series of the FTIR retrieved O_3 total column (bottom), as well as the partial column between surface and 20 km (middle) and the partial column between 20 and 40 km (top) from June 2018 to December 2019 at Xianghe. The grey dots are each individual retrieval. The orange dots and errorbars are the monthly means and STDs. The red dashed line is the mean and red solid line is the fitted seasonal variation. N is the measurement number.

partial column between surface and 20 km is $1.3 \times 10^{18}\mathrm{molecules/cm^2}$, which is much larger than that in the partial column between 20 and 40 km of $0.4 \times 10^{18}\mathrm{molecules/cm^2}$. Therefore, the seasonal variation of the total column is dominated by the lower partial column (surface-20 km). The FTIR O_3 retrieved lower partial column (surface-20 km) has a maximum sensitivity in the UTLS region (see Figure 2). The ozonesonde measurements between 2002 and 2010 at Beijing (Wang et al., 2012) showed that the high O_3 concentrations are in the UTLS in later winter and spring with a year-to-year variation, and the low O_3 concentrations in the UTLS in August-September. In the middle and upper stratosphere (20-40 km), the maximum observed in summer is mainly due to the higher photochemical production in this season (Perliski et al., 1989).

3 Validation of O_3 total and partial columns

On the purpose of validating the FTIR O_3 retrievals at Xianghe in the 3040 cm^{-1} spectral range, we first compare them with nearby ozonesonde and co-located TROPOMI measurements. Secondly, we apply the same retrieval strategy (3040 cm^{-1}) to the FTIR observations at the Maïdo (Reunion Island) which is a NDACC affiliated site, and we compare them with the standard NDACC O_3 retrievals (1000 cm^{-1}) at this site, as well as with nearby ozonesonde and co-located TROPOMI measurements.

3.1 Ozonesonde

The ozonesonde is a compact, lightweight balloon-borne instrument, which is coupled to a meteorological radiosonde. The balloon is launched at the surface and ascends up to the upper stratosphere (about 35 km), providing in-situ measurements of the ozone profile with a high vertical resolution of about few hundred meters (Thompson et al., 2003). According to Deshler et al. (2017), the accuracy of the ozonesonde profile is within 10% in the troposphere and 5% in the stratosphere. The precision of the ozonesonde is about 3-5% (Deshler et al., 2008; Liu et al., 2009).

The ozonesondes are launched at Beijing Observatory (39.81°N, 116.47°E, 31 m a.s.l.), about 50 km west of the Xianghe site. The ozonesonde instrument was developed at IAP, CAS (named as IAP ozonesonde). The IAP ozonesonde consists of an anode cell and a cathode cell, and uses an electrochemical method, which is similar to the Electrochemical Concentration Cell (ECC) type ozonesonde. For the detailed information about instrument, please refer to Zhang et al. (2014b). The performance of the IAP ozonesonde measurements has been evaluated by comparison with other ECC ozonesonde measurements (Zhang et al., 2014b): the average difference in the ozone partial pressure between the IAP and ECC ozonesondes is 0.3 mPa from the surface to 2.5 km, close to zero from 2.5 to 9 km and generally less than 1 mPa for layers higher than 9 km, and the precision of the IAP ozonsonde is within 5% in the troposphere and within 10% in the stratosphere, respectively. Note that we have applied the pressure pump efficiency corrections to the IAP ozonesonde (Zheng et al., 2018)~~, resulting in higher ozone detecting performance relative to the results in Zhang et al. (2014b)~~. The IAP ozonesonde measurements used in this study cover the period between June 2018 and February 2019, after which the ozonesonde measurements stopped.

The ozonesonde data performed at Gillot, Reunion Island (20.89°S, 55.53°E, 8 m a.s.l.) are affiliated to the NDACC ~~(De Maziere et al., 2008)~~ (De Mazière et al., 2018) and the Southern Hemisphere Additional Ozonesondes (SHADOZ) network (Thompson et al., 2003). Detailed information about the ozonesonde measurements at Gillot can be found in Thompson et al. (2014); Witte et al. (2017), where the ozonesonde measurements are applied to understand the tropospheric ozone increases over the southern Africa region. Gillot is about 26 km away from Maïdo, and is considered representative for the ozone concentrations at Maïdo (Duflot et al., 2017). The ozonesonde measurements used in this study cover the period between April 2013 and July 2017.

We select FTIR measurements within a $\pm$ 3-hours window around each ozonesonde, and take the averaged FTIR retrieval and the ozonesonde measurement as one FTIR-sonde data pair. In total, we have 16 and 53 data pairs at Xianghe and Maïdo, respectively. As the vertical resolution of ozonesondes is much higher than that of the FTIR retrievals, the ozonesonde profiles are smoothed with the FTIR averaging kernel to reduce the smoothing error in the comparison between both (Rodgers and

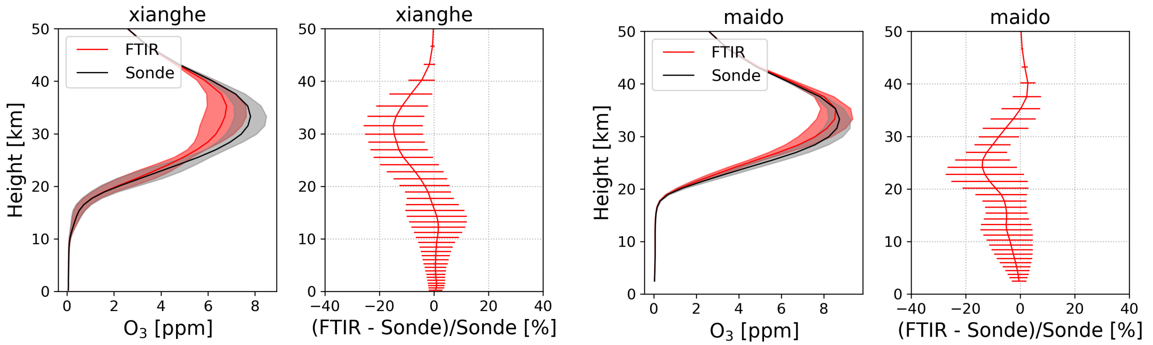

Figure 4. The O_3 profiles from the smoothed ozonesonde and FTIR retrievals (the solid line is the mean and the shadow is the STD), together with their relative differences (the solid line is the mean and the errorbar is the STD) at Xianghe (left) and Maïdo (right).

Connor, 2003):

$$\boldsymbol{x_s}' = \boldsymbol{x_{F,a}} + \mathbf{A}(\boldsymbol{x_s} - \boldsymbol{x_{F,a}}), \tag{4}$$

where $\boldsymbol{x_{F,a}}$ is the FTIR a priori profile, $\boldsymbol{x_s}$ is the ozonesonde profile, $\boldsymbol{x_s}'$ is the smoothed ozonesonde profile, and $\mathbf{A}$ is the FTIR averaging kernel. To apply the smoothing correction, we have extended the ozonesonde profile to the top of atmosphere using the FTIR a priori profile.

The profiles of the FTIR retrievals and ozonesonde measurements, together with their relative differences at Xianghe and Maïdo are shown in Figure 4. In general, the relative difference profiles at these two sites are similar: within $\pm$15% below 20 km and between -30 % and 10% between 20 km and 40 km. The total column observed by ozonesonde is 6.4 $\pm$ 6.0 (1σ) % and 9.0 $\pm$ 4.3 % larger than the FTIR (3040 cm^{-1}) retrievals at Xianghe and Maïdo, respectively. To check the impact of the O_3 columns above the maximum height of the ozonesonde, we also compare the FTIR column between the surface to the maximum altitude of each co-located ozonesonde profile, where the ozonesonde measurements are 6.2 $\pm$ 6.1 % and 9.7 $\pm$ 7.0 % larger than the FTIR retrievals at Xianghe and Maïdo, respectively. As a result, the impact of extending the ozonesonde profile to higher altitude with the FTIR a priori profile is relatively small compared to the large uncertainty. The comparisons between the total and partial columns (surface-20 km and 20-40 km) retrieved from the FTIR and the ozonesonde measurements are listed in Table 3.

3.2 TROPOMI satellite measurements

The Sentinel-5 Precursor (S5P) satellite, carrying the TROPOMI instrument, was successfully launched into a sun-synchronous orbit on 13 October 2017, providing a high horizontal resolution of 7$\times$3.5 km^2 before 6 August 2019 and of 5.5$\times$3.5 km^2 since then. TROPOMI observes a number of trace species globally, including O_3, with a nadir view. In this section, the TROPOMI offline (OFFL) total ozone column measurements are compared with the FTIR O_3 (3040 cm^{-1}) retrievals at Xianghe and Maïdo. The pre-launch requirements regarding accuracy and precision of the TROPOMI OFFL O_3 total column product are

Table 3. The mean and STD (mean/STD) of the relative differences between the FTIR O_3 (3040 cm^{-1}) retrievals with other datasets (ozonesonde, TROPOMI and FTIR O_3 (1000 cm^{-1} retrievals)) in total column and two partial columns (surface-20 km and 20-40 km) at Xianghe and Maïdo. The relative difference is calculated as (FTIR-other)/other × 100%.

	Datasets	Xianghe mean/std [%]	Maïdo mean/std [%]
Total column	Ozonesonde	-6.4/6.0	-9.0/4.3
	FTIR (1000 cm^{-1})		-8.4/1.1
	TROPOMI	-5.5/2.0	-6.1/1.3
Surface-20 km	Ozonesonde	-0.3/6.0	-2.4/6.6
	FTIR (1000 cm^{-1})		0.8/4.4
20-40 km	Ozonesonde	-10.3/7.8	-10.1/6.5
	FTIR (1000 cm^{-1})		-10.8/1.8

3.5-5.0% and 1.6-2.5%, respectively. TROPOMI OFFL O_3 total column products have been validated by ground-based Brewer, Dobson and Zenith Scattered Light-Differential Optical Absorption Spectroscopy (ZSL-DOAS) measurements. It is found that the mean bias between the TROPOMI and ground-based measurements is +0.1% and the STD of the relative differences is about 2.0%, which is within the mission requirements (Garane et al., 2019).

We select TROPOMI satellite OFFL data within a ± 6 hours temporal window and within a ± 1.0 ° latitude and ± 3.0 ° longitude box of each FTIR O_3 measurement at Xianghe and Maïdo. As the FTIR measurements at Xianghe start in June 2018, in this ~~study~~section, we compare the FTIR O_3 (3040 cm^{-1}) measurements with TROPOMI OFFL data between June 2018 and December 2019 at both sites. As mentioned in Section 2.1, the FTIR a priori profile is derived from the WACCM model, while the a priori profile of the TROPOMI retrieval is from a column-classified ozone profile climatology (Heue et al., 2018). In order to reduce the influence of different a priori profiles, we substitute the satellite a priori profile for the ground-based FTIR a priori profile when comparing both datasets

$$\boldsymbol{x}_r' = \boldsymbol{x}_r + (\mathbf{I} - \mathbf{A})(\boldsymbol{x}_{s,a} - \boldsymbol{x}_{F,a}), \tag{5}$$

where $\boldsymbol{x}_r'$ is the adapted FTIR profile by using satellite a priori profile as the a priori profile; $\boldsymbol{x}_r$ is the original FTIR retrieved profile; $\boldsymbol{x}_{s,a}$ and $\boldsymbol{x}_{F,a}$ are the satellite and FTIR a priori profiles. TROPOMI provides the column averaging kernel ($\boldsymbol{A_s}$) together with the total column, therefore, we applied the smoothing correction to the adapted FTIR profile:

$$TC_r' = TC_{s,a} + \boldsymbol{A_s PC_{dry,air}}(\boldsymbol{x}_r' - \boldsymbol{x}_{s,a}), \tag{6}$$

where $TC_{s,a}$ is the TROPOMI a priori total column and TC_r' is the FTIR retrieved total column after a priori profile substitution and taking TROPOMI vertical sensitivity into account.

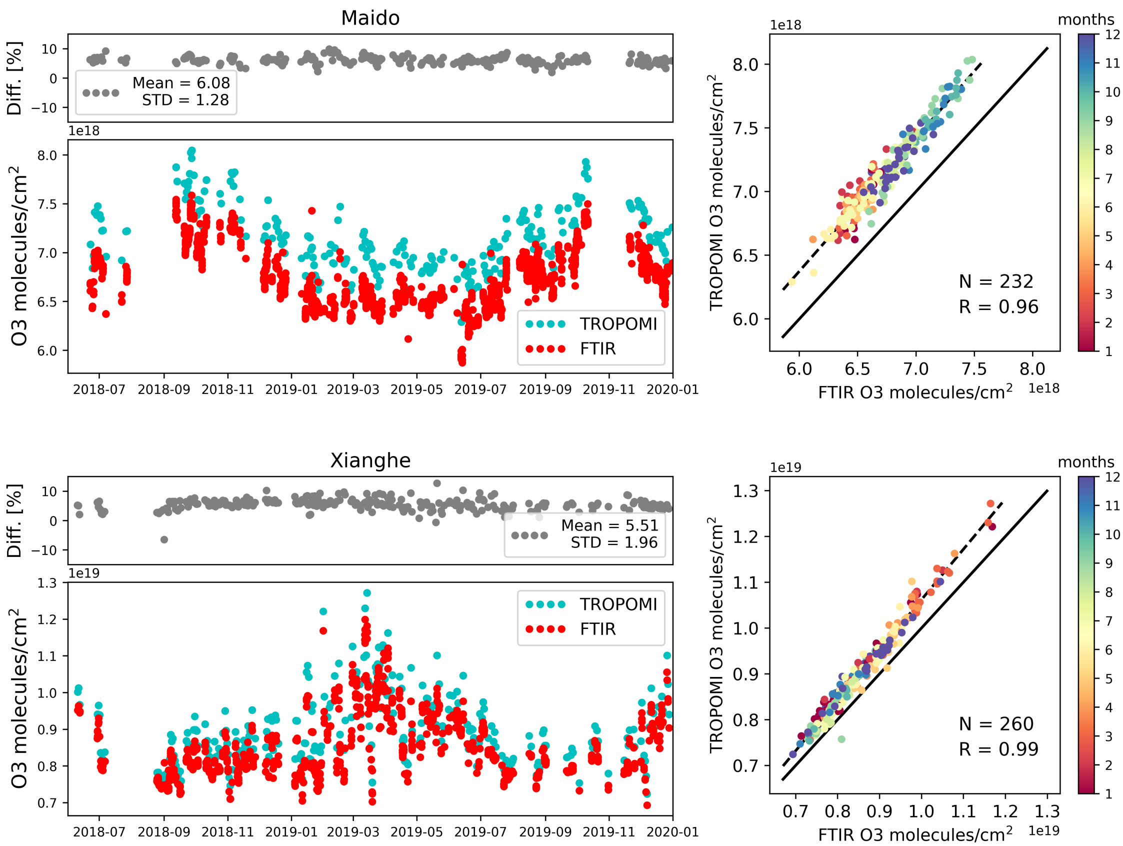

Figure 5. The time series of the co-located total columns from FTIR and TROPOMI measurements, together with their relative differences ((FTIR - TROPOMI)/TROPOMI $\times$ 100 %) and their correlations at Maïdo and Xianghe between June 2018 and December 2019. N is the co-located number of data pairs and R is the correlation coefficient. The correlation dots are coloured with their measurement months. The black dashed line is the linear regression line.

Figure 5 shows the time series of the co-located FTIR and TROPOMI O_3 total columns, together with their differences and correlations at Maïdo and Xianghe. Similar to ozonesonde measurements, the TROPOMI measurements are 5.5 $\pm$ 2.0 % and 6.1 $\pm$ 1.3 % larger than the FTIR (3040 cm^{-1}) total columns at Xianghe and Maïdo, respectively. In addition, there is no clear time dependence in the relative differences between FTIR and TROPOMI total columns.

There is a good correlation between the FTIR and TROPOMI measurements at Xianghe (R=0.99) and Maïdo (R=0.96). The seasonal and synoptic variations (phase and amplitude) of total columns of O_3 from the FTIR and TROPOMI measurements are very close to each other at both sites. As an example, FTIR and TROPOMI measurements show that there is a large enhancement of O_3 total column on 31 January 2019 at Xianghe (see Figure 6). Keep in mind that we should focus on the total column and two partial columns of FTIR measurements instead of the FTIR retrieved O_3 profile due to its limited vertical

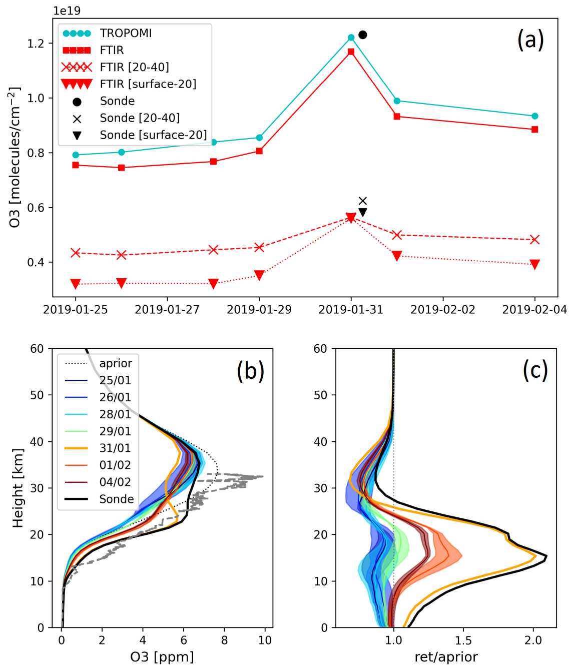

Figure 6. (a) ~~:~~the time series of the total and partial columns daily means from co-located FTIR and TROPOMI measurements between 25 January 2019 and 4 February 2019, and one ozonesonde profile (with smoothing using FTIR averaging kernel), on 31 January 2019 at Xianghe. For visualizing, the ozonesonde measurement is shifted by 6 hours. (b) ~~:~~the FTIR a priori (grey dot line) and retrieved (colored with date) profiles during this period. The shadow is the STD of the retrieved profile for each day. The grey dashed line is the original ozonesonde profile, and the ~~back~~ black solid line is the smoothed ozonesonde profile. (c) ~~:~~the ratios of the FTIR retrieved profiles and the smoothed ozonesonde profile to the FTIR a priori profile.

information. According to the FTIR measurements, both partial columns increase on that day, but the large increase of the total column mainly results from the enhancement of the lower partial column from the surface to 20 km altitude. There is one ozonesonde profile available on 31 January 2019, which confirms that the O_3 mole fraction is much larger compared to the FTIR a priori profile above 10 km, especially in the UTLS region. The smoothed ozonesonde profile is close to the FTIR retrieved profile below 23 km, which is consistent with our results in Table 3.

3.3 FTIR (1000 cm^{-1}) retrievals

Maïdo is an NDACC station, where FTIR measurements using ~~a~~ an MCT detector are carried out (Baray et al., 2013; Zhou et al., 2018). The harmonized O_3 standard retrieval strategy using 1000-1005 cm^{-1} has been performed at Maïdo, so that we can compare the FTIR (3040 cm^{-1}) with the FTIR (1000 cm^{-1}) retrievals for total column as well as for two partial columns. The FTIR O_3 (1000 cm^{-1}) retrieval has a DOFS of about 4 to 5, because in this spectral range it benefits from more O_3 lines with different intensities. The systematic and random uncertainties of the total column from FTIR O_3 (1000 cm^{-1})

retrievals are about 3.0% and 1.0%, respectively. The systematic and random uncertainties of the surface to 20 km partial column retrievals are about 3.2% and 2.5%, respectively, and of the 20 to 40 km partial column retrievals are about 3.4% and 1.5%, respectively. Both precision and accuracy are better using O_3 (1000 cm^{-1}) than O_3 (3040 cm^{-1}), which explains why the MCT spectral region is preferred at NDACC stations where these measurements are available. The systematic uncertainty is also dominated by the spectroscopy (HITRAN2008; Rothman et al. (2009)), where we set 3% for the uncertainty of line intensity (NDACC-IRWG recommendation, based on total column comparisons with Dobson and Brewer measurements, e.g. in Vigouroux et al. (2008)).

The a priori profiles of the FTIR O_3 (1000 cm^{-1}) retrievals are the same as those of the FTIR O_3 (3040 cm^{-1}) retrievals (see Section 2.1). To take the low vertical resolution of the FTIR (3040 cm^{-1}) retrieval into account, the FTIR (1000 cm^{-1}) retrieved profile is smoothed with the FTIR (3040 cm^{-1}) averaging kernel

$$\boldsymbol{x_{1000}}' = \boldsymbol{x_a} + \mathbf{A}(\boldsymbol{x_{1000}} - \boldsymbol{x_a}), \tag{7}$$

where $\boldsymbol{x_a}$ is the FTIR a priori profile; $\boldsymbol{x_{1000}}$ is the FTIR (1000 cm^{-1}) retrieved profile, $\boldsymbol{x_{1000}}'$ is the FTIR (1000 cm^{-1}) retrieved profile after smoothing with the FTIR (3040 cm^{-1}) averaging kernel ($\mathbf{A}$).

The time series of the hourly means retrieved O_3 total column and partial columns (surface-20 km and 20-40 km) in the 3040 cm^{-1} and 1000 cm^{-1} spectral ranges, together with their differences and correlations are shown in Figure 7. Both O_3 datasets show the same seasonal variations in the total column and the two partial columns. The mean and STD of their relative differences are also listed in Table 3. The O_3 (3040 cm^{-1}) total columns have a negative bias of 8.4 $\pm$ 1.1 % compared to the O_3 (1000 cm^{-1}) total columns. For the lower partial column (surface-20 km), the two FTIR O_3 retrievals are close to each other, with a mean relative difference of 0.8 $\pm$ 4.4 %. The O_3 upper partial column (20-40 km) retrieved in the 3040 cm^{-1} spectral range is 10.8 $\pm$ 1.8 % smaller than the one retrieved in the 1000 cm^{-1} spectral range.

García et al. (2014) found that there is an underestimation of 7% in the FTIR O_3 (3040 cm^{-1}) total column compared to FTIR O_3 (1000 cm^{-1}) retrievals at Izaña based on the HITRAN2012 spectroscopy (Rothman et al., 2013), which is generally in good agreement with our result (8.4 $\pm$ 1.1 %) at Maïdo. In this study, we also looked at comparisons between the two partial columns. The biases observed between FTIR O_3 (3040 cm^{-1}) and FTIR O_3 (1000 cm^{-1}) on one hand and between FTIR O_3 (3040 cm^{-1}) and ozonesondes on the other hand are similar (see Table 3), pointing to an underestimation of the FTIR retrieved total and partial columns products in the 3040 cm^{-1} spectral range; the bias is coming mainly from the 20-40 km partial column bias.

The FTIR O_3 (3040 cm^{-1}) retrievals and the FTIR O_3 (1000 cm^{-1}) retrievals are highly correlated, with R values of 0.95, 0.87 and 0.89 in the total column, the lower partial column (surface-20 km) and the upper partial column (20-40 km), respectively. The mean of daily STDs for the days for which more than 4 measurements are available are 0.57% and 0.58% in the total column, 2.41% and 0.85% in the lower partial column (surface-20 km), and 0.77% and 0.71% in the upper partial column (20-40 km) for FTIR O_3 (3040 cm^{-1}) and smoothed FTIR O_3(1000 cm^{-1}) retrievals, respectively. In summary, the two FTIR O_3 retrievals at Maïdo show a similar precision in the total column and the upper partial column (20-40 km), while

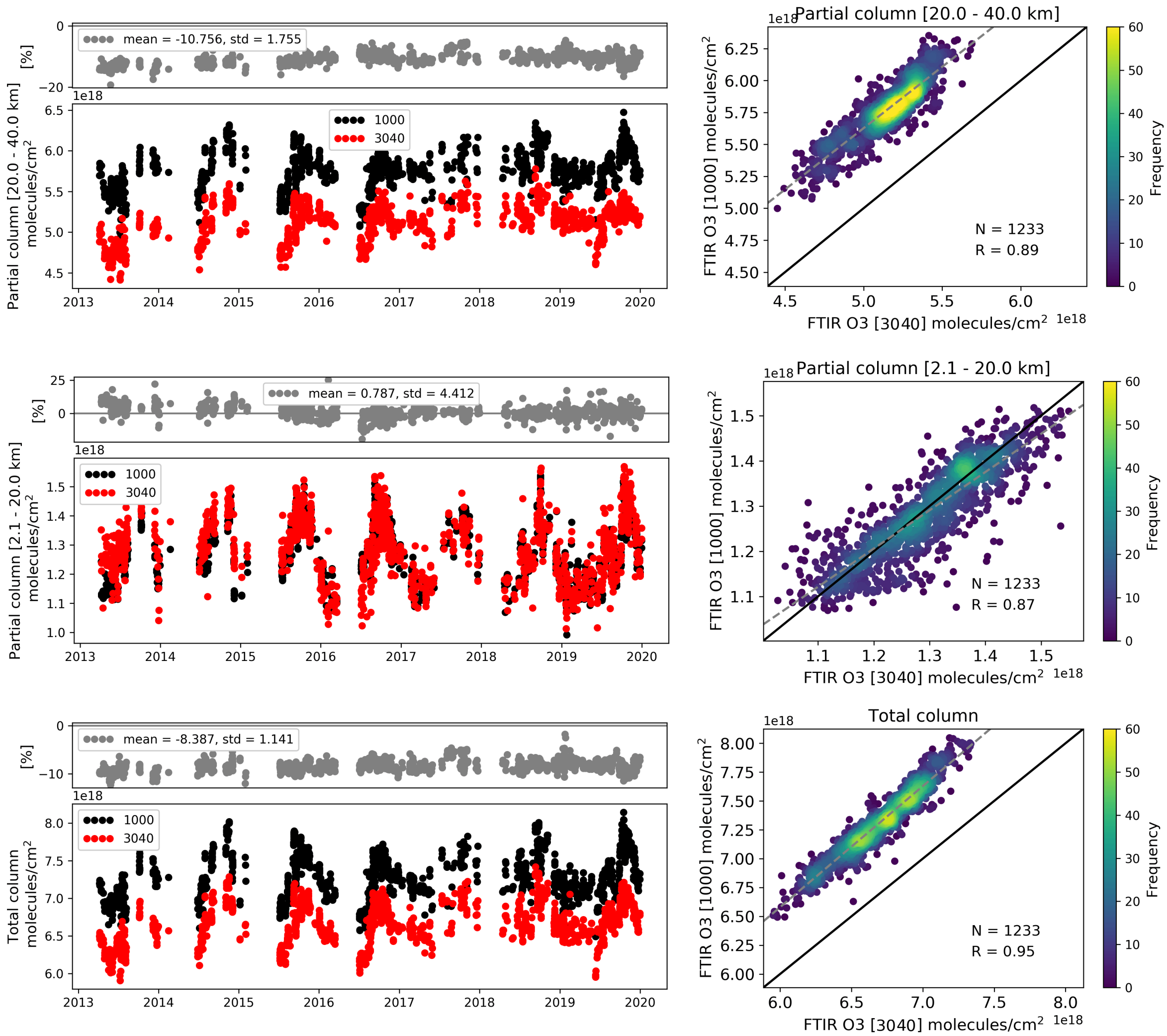

Figure 7. The time series of the co-located hourly means of total columns (bottom), partial columns between surface and 20 km (middle) and partial columns between 20 and 40 km (top) from FTIR retrievals using the 3040 cm^{-1} (red) and the 1000 cm^{-1} (black) spectral ranges, together with their relative differences ((FTIR_3040 - FTIR_1000)/FTIR_1000 × 100 %) and their correlations, in which color intensity corresponds to data frequency, at Maïdo between 2013 and 2019. The grey dashed line is the linear regression line. N is the co-located number of data pairs and R is the correlation coefficient.

the FTIR O_3 lower partial columns (surface-20 km) retrievals are more variable in the 3040 cm^{-1} than in the 1000 cm^{-1} spectral range.

4 Conclusions

The standard NDACC-IRWG O_3 retrieval uses the retrieval window of 1000-1005 cm^{-1} recorded with ~~a~~ an MCT detector. However at some ground-based atmospheric observatories the FTIR solar absorption instruments are not configured for operation with ~~a~~ an MCT detector. This is the case at Xianghe, China (39.75 °N, 116.96 °E), where the FTIR instrument is operated with InSb and InGaAs detectors covering the spectral range from 1800 cm^{-1} to 11000 cm^{-1}. Therefore, in this paper, we present ground-based FTIR O_3 retrievals at Xianghe between June 2018 and December 2019 using the standard NDACC-IRWG SFIT4 v9.4.4 retrieval algorithm and the spectral windows (3039.9 - 3040.6 cm^{-1}, 3041.5 - 3042.25 cm^{-1} and 3044.7 - 3045.54 cm^{-1}). The resulting averaging kernel shows that the retrieved O_3 profile is mainly sensitive to the vertical range between ~~5~~ 10 and 40 km, and the DOFS is 2.4±0.3 (1σ), indicating that we can retrieve two independent partial columns, one from the surface to 20 km and a second one from 20 to 40 km altitude. Based on the optimal estimation method, we have estimated the systematic and random uncertainties of the retrieved FTIR O_3 total columns to be about 13.6% and 1.4%, respectively, in which the random error is generally in good agreement with the observed daily STD of the FTIR retrievals.

The FTIR retrieval systematic uncertainty is then verified by comparing the FTIR O_3 retrievals in the 3040 cm^{-1} spectral range with nearby ozonesonde and co-located TROPOMI measurements at Xianghe and Maïdo, and with NDACC standard FTIR O_3 (1000 cm^{-1}) retrievals at Maïdo. There is a systematic underestimation by 5.5-9.0% in the FTIR O_3 (3040 cm^{-1}) total column retrievals, which is within the estimated systematic uncertainty and mainly due to the spectroscopic uncertainties. According to ozonesonde measurements and standard NDACC FTIR O_3 retrievals, the underestimation of the FTIR (3040 cm^{-1}) O_3 total column mainly results from the underestimation by 10.1-10.8% in the upper partial column (20-40 km). The systematic uncertainty is relatively small in the lower partial column (surface-20 km), which is within 2.4%.

At Xianghe, the FTIR retrieved O_3 partial columns between surface and 20 km show a maximum in February-April and a minimum in August-September, with a peak-to-peak amplitude of 1.3×10^{18}molecules/cm^2, while the 20-40 km partial columns show a maximum in May-July and a minimum in October-December, with a peak-to-peak amplitude of 0.4×10^{18}molecules/cm^2. As the amplitude of the seasonal variation in the lower partial column (surface-20 km) is much larger than the one in the upper partial column (20-40 km), the seasonal variation of the total column is dominated by the lower partial column. The FTIR (3040 cm^{-1}) retrievals at Xianghe and Maïdo show the same seasonal and synoptic O_3 variations as seen by the TROPOMI satellite measurements and the NDACC standard FTIR O_3 retrievals at Maïdo.

The ongoing FTIR O_3 total and partial columns (surface-20 km and 20-40 km) data at Xianghe can provide useful information on O_3 synoptic and seasonal variations and long-term trends. Based on the successful and consistent O_3 retrieved results at Xianghe and Maïdo, the retrieval strategy used in this study can be extended to other FTIR sites recording the 3040 cm^{-1} spectral range.

Data availability. The NDACC standard FTIR O_3 (1000 cm^{-1}) retrievals at Maïdo and the ozonesonde measurements are publicly available at the NDACC archive (ftp://ftp.cpc.ncep.noaa.gov/ndacc/; last access: 20 January 2019). The TROPOMI off-line data are publicly available at ESA Copernicus Open Access Hub (https://scihub.copernicus.eu/). The ozonesonde and FTIR O_3 (3040 cm^{-1}) retrievals at Xianghe used in this study can be obtained by contacting the authors.

Appendix A: FTIR O_3 (3040 cm^{-1}) retrieval window

The retrieval windows used in this study are modified from the 3040 cm^{-1} recipe of García et al. (2014). As mentioned in Section 2.1, the windows 2 and 3 are taken from their recipe but we use the window 1 (3039.9-3040.6 cm^{-1}) instead of the window between 3042.48 and 3043.72 cm^{-1} to reduce the impact from water vapor. To better understand the influence of retrieval window, we also perform the FTIR O_3 retrieval at Xianghe using the window in García et al. (2014) (3041.47-3045.66 cm^{-1} with disregarding the residuals in the 3042.28-3042.48 cm^{-1} and 3043.72-3044.04 cm^{-1} ranges), and keep other settings same as the retrieval strategy described in Section 2.1. Note that the columns of interfering species (CH_4, HCl, $H_2^{18}O$, $H_2^{17}O$, H_2O, HDO, and CO_2) are retrieved simultaneously. Figure A1 shows the observed and fitted transmittances between 3042.48 and 3043.72 cm^{-1} of the same spectrum shown in Figure 1, containing several absorption lines of water vapor. It is noticed that the CH_4 lines are not well fitted in this region so that the RMS of the residual in this region is about 20% larger as compared to the windows used in this study. Figure A2 shows the time series and the correlation plot of the FTIR retrieved O_3 total columns using the windows in this study and the García's window at Xianghe. The mean and standard deviation of the relative difference (this study-García) are 0.8% and 1.2%, and the correlation coefficient is 0.99, indicating that the two FTIR O_3 retrieved total columns are close to each other. However, the number of the successfully retrieved spectra using the windows in this study is 937, which is larger than the number of 895 using the García's choice, especially in summer with high humidity. Besides, the mean of the daily standard deviation of the retrieved total column for all days with more than 4 measurements using the García's window is 1.4%, which is slightly larger as compared to 1.3% using the windows in this study. Therefore, we use the window (3039.9-3040.6 cm^{-1}) instead of the window (3042.48-3043.72 cm^{-1}), which gives us a better result at Xianghe.

Competing interests. The authors declare that they have no conflict of interest.

Acknowledgements. This research was funded by the National Key R&D Program of China (Nos. 2017YFB0504000 and 2017YFC1501701) and the National Natural Science Foundation of China (41975035). The FTIR site at Reunion Island are operated by the BIRA-IASB and locally supported by LACy/UMR8105, Université de La Réunion. We would like to thank Weidong Nan, Qun Cheng and Rongshi Zou (IAP) for the FTIR maintenance at Xianghe, Geoffrey C. Toon (JPL, NASA) for sharing the ATM2019 spectroscopy, Daan Hubert (BIRA-IASB) for useful discussion about the ozonesonde measurements, and Ball William (ETH zürich) for useful discussions. We also acknowledge the NDACC-IRWG network for providing the retrieval code and data, and ESA for providing the TROPOMI products. The work done by MZ and BIRA colleagues has been supported through the Copernicus Atmospheric Monitoring Service contracts (CAMS-84 and CAMS-27).

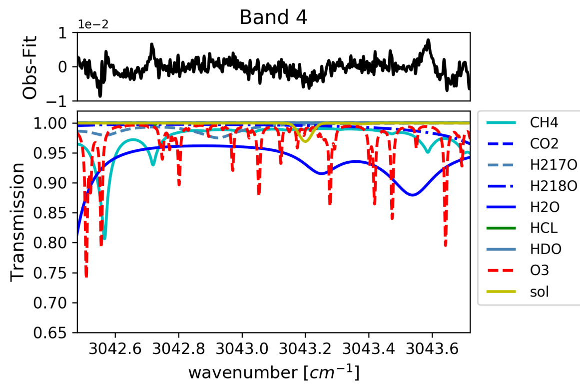

Figure A1. An example of spectral fit in the microwindow between 3042.48 and 3043.72 cm^{-1} using the recipe of García et al. (2014) at Xianghe. It is the same spectrum shown in Figure 1. Lower panel: the normalized transmittance from each atmospheric species and solar lines. Upper panel: the difference between the observed and fitted spectra (Obs-Fit).

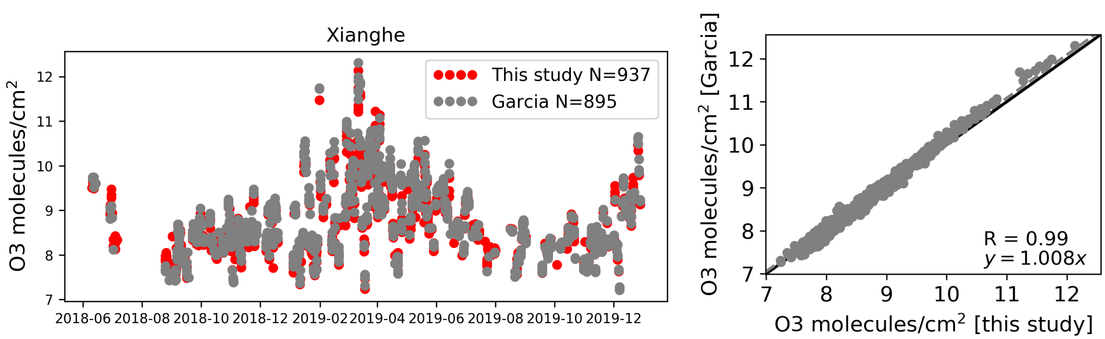

Figure A2. The time series the FTIR retrieved O_3 total column using the windows in this study and García's choice at Xianghe (left), together with their correlation (right).

Author contributions. MZ wrote the manuscript. MZ and PW designed the experiment, with the significant inputs from BL, CV, LR, MDM. CH, NK, TW, YY, DJ, JMM collected the FTIR measurements at Xianghe and Maïdo. JZ, YX, HC, VD, FP provided and studied the ozonesonde measurements at Beijing and Gillot. All the authors read and commented on the manuscript.

References

Baray, J. L., Courcoux, Y., Keckhut, P., Portafaix, T., Tulet, P., Cammas, J. P., Hauchecorne, A., Godin Beekmann, S., De Mazière, M., Hermans, C., Desmet, F., Sellegri, K., Colomb, A., Ramonet, M., Sciare, J., Vuillemin, C., Hoareau, C., Dionisi, D., Duflot, V., Vérèmes, H., Porteneuve, J., Gabarrot, F., Gaudo, T., Metzger, J. M., Payen, G., Leclair De Bellevue, J., Barthe, C., Posny, F., Ricaud, P., Abchiche, A., and Delmas, R.: Maïdo observatory: A new high-altitude station facility at Reunion Island (21 S, 55 E) for long-term atmospheric remote sensing and in situ measurements, Atmos. Meas. Tech., 6, 2865–2877, https://doi.org/10.5194/amt-6-2865-2013, 2013.

Boynard, A., Hurtmans, D., Garane, K., Goutail, F., Hadji-Lazaro, J., Koukouli, M. E., Wespes, C., Vigouroux, C., Keppens, A., Pommereau, J.-P., Pazmino, A., Balis, D., Loyola, D., Valks, P., Sussmann, R., Smale, D., Coheur, P.-F., and Clerbaux, C.: Validation of the IASI FORLI/EUMETSAT ozone products using satellite (GOME-2), ground-based (Brewer–Dobson, SAOZ, FTIR) and ozonesonde measurements, Atmos. Meas. Tech., 11, 5125–5152, https://doi.org/10.5194/amt-11-5125-2018, 2018.

De Maziere, M., Vigouroux, C., Bernath, P. F., Baron, P., Blumenstock, T., Boone, C., Brogniez, C., Catoire, V., Coffey, M., Duchatelet, P., Griffith, D., Hannigan, J., Kasai, Y., Kramer, I., Jones, N. B., Mahieu, E., Manney, G. L., Piccolo, C., Randall, C., Robert, C., Senten, C., Strong, K., Taylor, J., Tetard, C., Walker, K. a., and Wood, S.: Validation of ACE-FTS v2.2 methane profiles from the upper troposphere to the lower mesosphere, Atmos. Chem. Phys, 8, 2421–2435, https://doi.org/10.5194/acp-8-2421-2008, www.atmos-chem-phys.net/8/2421/2008/, 2008.

De Mazière, M., Thompson, A. M., Kurylo, M. J., Wild, J. D., Bernhard, G., Blumenstock, T., Braathen, G. O., Hannigan, J. W., Lambert, J.-C., Leblanc, T., McGee, T. J., Nedoluha, G., Petropavlovskikh, I., Seckmeyer, G., Simon, P. C., Steinbrecht, W., and Strahan, S. E.: The Network for the Detection of Atmospheric Composition Change (NDACC): history, status and perspectives, Atmos. Chem. Phys., 18, 4935–4964, https://doi.org/10.5194/acp-18-4935-2018, 2018.

Deshler, T., Mercer, J. L., Smit, H. G., Stubi, R., Levrat, G., Johnson, B. J., Oltmans, S. J., Kivi, R., Thompson, A. M., Witte, J., Davies, J., Schmidlin, F. J., Brothers, G., and Sasaki, T.: Atmospheric comparison of electrochemical cell ozonesondes from different manufacturers, and with different cathode solution strengths: The Balloon Experiment on Standards for Ozonesondes, J. Geophys. Res. Atmos., 113, https://doi.org/10.1029/2007JD008975, 2008.

Deshler, T., Stübi, R., Schmidlin, F. J., Mercer, J. L., Smit, H. G. J., Johnson, B. J., Kivi, R., and Nardi, B.: Methods to homogenize electrochemical concentration cell (ECC) ozonesonde measurements across changes in sensing solution concentration or ozonesonde manufacturer, Atmos. Meas. Tech., 10, 2021–2043, https://doi.org/10.5194/amt-10-2021-2017, 2017.

Duflot, V., Baray, J.-L., Payen, G., Marquestaut, N., Posny, F., Metzger, J.-M., Langerock, B., Vigouroux, C., Hadji-Lazaro, J., Portafaix, T., De Mazière, M., Coheur, P.-F., Clerbaux, C., and Cammas, J.-P.: Tropospheric ozone profiles by DIAL at Maïdo Observatory (Reunion Island): system description, instrumental performance and result comparison with ozone external data set, Atmos. Meas. Tech., 10, 3359–3373, https://doi.org/10.5194/amt-10-3359-2017, 2017.

European Commission, .: Emission Database for Global Atmospheric Research (EDGAR), release EDGARv4.2 FT2010, Tech. rep., Joint Research Centre (JRC)/Netherlands Environmental Assessment Agency (PBL). last access: 12 April 2020, http://edgar.jrc.ec.europa.eu, 2013.

Feng, Z., De Marco, A., Anav, A., Gualtieri, M., Sicard, P., Tian, H., Fornasier, F., Tao, F., Guo, A., and Paoletti, E.: Economic losses due to ozone impacts on human health, forest productivity and crop yield across China, Environ. Int., 131, 104 966, https://doi.org/10.1016/J.ENVINT.2019.104966, 2019.

Garane, K., Koukouli, M.-E., Verhoelst, T., Lerot, C., Heue, K.-P., Fioletov, V., Balis, D., Bais, A., Bazureau, A., Dehn, A., Goutail, F., Granville, J., Griffin, D., Hubert, D., Keppens, A., Lambert, J.-C., Loyola, D., McLinden, C., Pazmino, A., Pommereau, J.-P., Redondas, A., Romahn, F., Valks, P., Van Roozendael, M., Xu, J., Zehner, C., Zerefos, C., and Zimmer, W.: TROPOMI/S5P total ozone column data: global ground-based validation and consistency with other satellite missions, Atmos. Meas. Tech., 12, 5263–5287, https://doi.org/10.5194/amt-12-5263-2019, 2019.

García, O. E., Schneider, M., Hase, F., Blumenstock, T., Sepúlveda, E., and González, Y.: Quality assessment of ozone total column amounts as monitored by ground-based solar absorption spectrometry in the near infrared (> 3000 cm-1), Atmos. Meas. Tech., 7, 3071–3084, https://doi.org/10.5194/amt-7-3071-2014, 2014.

Heue, K.-P., Spurr, R., Loyola, D., Van Roozendael, M., Lerot, C., and Xu, J.: S5P/TROPOMI Total Ozone ATBD, S5P-L2-DLRATBD-400A, http://www.tropomi.eu/documents/atbd, 2018.

IPCC: Climate change 2013: The physical science basis. Contribution of Working Group I to the Fifth Assessment Report of the Intergovernmental Panel on Climate Change, 2013.

Langematz, U.: Stratospheric ozone: down and up through the anthropocene, ChemTexts, 5, 8, https://doi.org/10.1007/s40828-019-0082-7, 2019.

Lickley, M., Solomon, S., Fletcher, S., Velders, G. J. M., Daniel, J., Rigby, M., Montzka, S. A., Kuijpers, L. J. M., and Stone, K.: Quantifying contributions of chlorofluorocarbon banks to emissions and impacts on the ozone layer and climate, Nature Communications, 11, 1380, https://doi.org/10.1038/s41467-020-15162-7, 2020.

Lindenmaier, R., Batchelor, R. L., Strong, K., Fast, H., Goutail, F., Kolonjari, F., Thomas McElroy, C., Mittermeier, R. L., and Walker, K. A.: An evaluation of infrared microwindows for ozone retrievals using the Eureka Bruker 125HR Fourier transform spectrometer, J. Quant. Spectrosc. Radiat. Transf., 111, 569–585, https://doi.org/10.1016/j.jqsrt.2009.10.013, 2010.

Liu, G., Tarasick, D. W., Fioletov, V. E., Sioris, C. E., and Rochon, Y. J.: Ozone correlation lengths and measurement uncertainties from analysis of historical ozonesonde data in North America and Europe, J. Geophys. Res., 114, https://doi.org/10.1029/2008jd010576, 2009.

Ma, Z., Xu, J., Quan, W., Zhang, Z., Lin, W., and Xu, X.: Significant increase of surface ozone at a rural site, north of eastern China, Atmos. Chem. Phys., 16, 3969–3977, https://doi.org/10.5194/acp-16-3969-2016, 2016.

Molina, M. J. and Rowland, F. S.: Stratospheric sink for chlorofluoromethanes: chlorine atom-catalysed destruction of ozone, Nature, 249, 810–812, https://doi.org/10.1038/249810a0, 1974.

Monks, P. S., Archibald, A. T., Colette, A., Cooper, O., Coyle, M., Derwent, R., Fowler, D., Granier, C., Law, K. S., Mills, G. E., Stevenson, D. S., Tarasova, O., Thouret, V., von Schneidemesser, E., Sommariva, R., Wild, O., and Williams, M. L.: Tropospheric ozone and its precursors from the urban to the global scale from air quality to short-lived climate forcer, Atmos. Chem. Phys., 15, 8889–8973, https://doi.org/10.5194/acp-15-8889-2015, 2015.

Montzka, S. A., Butler, J. H., Myers, R. C., Thompson, T. M., Swanson, T. H., Clarke, A. D., Lock, L. T., and Elkins, J. W.: Decline in the Tropospheric Abundance of Halogen from Halocarbons: Implications for Stratospheric Ozone Depletion, Science, 272, 1318–22, https://doi.org/10.1126/science.272.5266.1318, 1996.

Montzka, S. A., Dutton, G. S., Yu, P., Ray, E., Portmann, R. W., Daniel, J. S., Kuijpers, L., Hall, B. D., Mondeel, D., Siso, C., Nance, J. D., Rigby, M., Manning, A. J., Hu, L., Moore, F., Miller, B. R., and Elkins, J. W.: An unexpected and persistent increase in global emissions of ozone-depleting CFC-11, Nature, 557, 413–417, 2018.

Murdoch, J. C. and Sandler, T.: The voluntary provision of a pure public good: The case of reduced CFC emissions and the Montreal Protocol, J. Public Econ., 63, 331–349, https://doi.org/10.1016/S0047-2727(96)01598-8, 1997.

Perliski, L. M., Solomon, S., and London, J.: On the interpretation of seasonal variations of stratospheric ozone, Planet. Space Sci., 37, 1527–538, https://doi.org/10.1016/0032-0633(89)90143-8, 1989.

Pougatchev, N. S., Connor, B. J., and Rinsland, C. P.: Infrared measurements of the ozone vertical distribution above Kitt Peak, J. Geophys. Res., 100, 16 689, https://doi.org/10.1029/95JD01296, 1995.

Rigby, M., Park, S., Saito, T., Western, L. M., Redington, A. L., Fang, X., Henne, S., Manning, A. J., Prinn, R. G., Dutton, G. S., Fraser, P. J., Ganesan, A. L., Hall, B. D., Harth, C. M., Kim, J., Kim, K. R., Krummel, P. B., Lee, T., Li, S., Liang, Q., Lunt, M. F., Montzka, S. A., Mühle, J., O'Doherty, S., Park, M. K., Reimann, S., Salameh, P. K., Simmonds, P., Tunnicliffe, R. L., Weiss, R. F., Yokouchi, Y., and Young, D.: Increase in CFC-11 emissions from eastern China based on atmospheric observations, Nature, 569, 546–550, https://doi.org/10.1038/s41586-019-1193-4, 2019.

Rodgers, C. D.: Inverse Methods for Atmospheric Sounding – Theory and Practice, Series on Atmospheric Oceanic and Planetary Physics, vol. 2, World Scientific Publishing Co. Pte. Ltd, Singapore, https://doi.org/10.1142/9789812813718, 2000.

Rodgers, C. D. and Connor, B. J.: Intercomparison of remote sounding instruments, J. Geophys. Res., 108, 46–48, https://doi.org/10.1029/2002JD002299, 2003.

Rothman, L. S., Gordon, I. E., Barbe, A., Benner, D. C., Bernath, P. F., Birk, M., Boudon, V., Brown, L. R., Campargue, A., Champion, J. P., Chance, K., Coudert, L. H., Dana, V., Devi, V. M., Fally, S., Flaud, J. M., Gamache, R. R., Goldman, A., Jacquemart, D., Kleiner, I., Lacome, N., Lafferty, W. J., Mandin, J. Y., Massie, S. T., Mikhailenko, S. N., Miller, C. E., Moazzen-Ahmadi, N., Naumenko, O. V., Nikitin, A. V., Orphal, J., Perevalov, V. I., Perrin, A., Predoi-Cross, A., Rinsland, C. P., Rotger, M., Šimečková, M., Smith, M. A., Sung, K., Tashkun, S. A., Tennyson, J., Toth, R. A., Vandaele, A. C., and Vander Auwera, J.: The HITRAN 2008 molecular spectroscopic database, J. Quant. Spectrosc. Radiat. Transf., 110, 533–572, https://doi.org/10.1016/j.jqsrt.2009.02.013, 2009.

Rothman, L. S., Gordon, I. E., Babikov, Y., Barbe, A., Chris Benner, D., Bernath, P. F., Birk, M., Bizzocchi, L., Boudon, V., Brown, L. R., Campargue, A., Chance, K., Cohen, E. A., Coudert, L. H., Devi, V. M., Drouin, B. J., Fayt, A., Flaud, J. M., Gamache, R. R., Harrison, J. J., Hartmann, J. M., Hill, C., Hodges, J. T., Jacquemart, D., Jolly, A., Lamouroux, J., Le Roy, R. J., Li, G., Long, D. A., Lyulin, O. M., Mackie, C. J., Massie, S. T., Mikhailenko, S., Müller, H. S. P., Naumenko, O. V., Nikitin, A. V., Orphal, J., Perevalov, V., Perrin, A., Polovtseva, E. R., Richard, C., Smith, M. A. H., Starikova, E., Sung, K., Tashkun, S., Tennyson, J., Toon, G. C., Tyuterev, V. G., and Wagner, G.: The HITRAN2012 molecular spectroscopic database, J. Quant. Spectrosc. Radiat. Transf., 130, 4–50, https://doi.org/10.1016/j.jqsrt.2013.07.002, 2013.

Steinbrecht, W., Froidevaux, L., Fuller, R., Wang, R., Anderson, J., Roth, C., Bourassa, A., Degenstein, D., Damadeo, R., Zawodny, J., Frith, S., McPeters, R., Bhartia, P., Wild, J., Long, C., Davis, S., Rosenlof, K., Sofieva, V., Walker, K., Rahpoe, N., Rozanov, A., Weber, M., Laeng, A., von Clarmann, T., Stiller, G., Kramarova, N., Godin-Beekmann, S., Leblanc, T., Querel, R., Swart, D., Boyd, I., Hocke, K., Kämpfer, N., Maillard Barras, E., Moreira, L., Nedoluha, G., Vigouroux, C., Blumenstock, T., Schneider, M., García, O., Jones, N., Mahieu, E., Smale, D., Kotkamp, M., Robinson, J., Petropavlovskikh, I., Harris, N., Hassler, B., Hubert, D., and Tummon, F.: An update on ozone profile trends for the period 2000 to 2016, Atmos. Chem. Phys., 17, 10 675–10 690, https://doi.org/10.5194/acp-17-10675-2017, 2017.

Takele Kenea, S., Mengistu Tsidu, G., Blumenstock, T., Hase, F., von Clarmann, T., and Stiller, G. P.: Retrieval and satellite intercomparison of O3 measurements from ground-based FTIR Spectrometer at Equatorial Station: Addis Ababa, Ethiopia, Atmos. Meas. Tech., 6, 495–509, https://doi.org/10.5194/amt-6-495-2013, 2013.

Thompson, A. M., Witte, J. C., McPeters, R. D., Oltmans, S. J., Schmidlin, F. J., Logan, J. A., Fujiwara, M., Kirchhoff, V. W., Posny, F., Coetzee, G. J., Hoegger, B., Kawakami, S., Ogawa, T., Johnson, B. J., Vömel, H., and Labow, G.: Southern Hemisphere Additional

Ozonesondes (SHADOZ) 1998-2000 tropical ozone climatology 1. Comparison with Total Ozone Mapping Spectrometer (TOMS) and ground-based measurements, J. Geophys. Res. D Atmos., 108, 8238, https://doi.org/10.1029/2001jd000967, 2003.

Thompson, A. M., Balashov, N. V., Witte, J. C., Coetzee, J. G. R., Thouret, V., and Posny, F.: Tropospheric ozone increases over the southern Africa region: bellwether for rapid growth in Southern Hemisphere pollution?, Atmos. Chem. Phys., 14, 9855–9869, https://doi.org/10.5194/acp-14-9855-2014, 2014.

Vigouroux, C., De Mazière, M., Demoulin, P., Servais, C., Hase, F., Blumenstock, T., Kramer, I., Schneider, M., Mellqvist, J., Strandberg, A., Velazco, V., Notholt, J., Sussmann, R., Stremme, W., Rockmann, A., Gardiner, T., Coleman, M., and Woods, P.: Evaluation of tropospheric and stratospheric ozone trends over Western Europe from ground-based FTIR network observations, Atmos. Chem. Phys., 8, 6865–6886, https://doi.org/10.5194/acp-8-6865-2008, 2008.

Vigouroux, C., Blumenstock, T., Coffey, M., Errera, Q., Garciá, O., Jones, N. B., Hannigan, J. W., Hase, F., Liley, B., Mahieu, E., Mellqvist, J., Notholt, J., Palm, M., Persson, G., Schneider, M., Servais, C., Smale, D., Thölix, L., and De Mazière, M.: Trends of ozone total columns and vertical distribution from FTIR observations at eight NDACC stations around the globe, Atmos. Chem. Phys., 15, 2915–2933, https://doi.org/10.5194/acp-15-2915-2015, 2015.

Wang, Y., Konopka, P., Liu, Y., Chen, H., Müller, R., Plöger, F., Riese, M., Cai, Z., and Lü, D.: Tropospheric ozone trend over Beijing from 2002–2010: ozonesonde measurements and modeling analysis, Atmos. Chem. Phys., 12, 8389–8399, https://doi.org/10.5194/acp-12-8389-2012, 2012.

Witte, J. C., Thompson, A. M., Smit, H. G., Fujiwara, M., Posny, F., Coetzee, G. J., Northam, E. T., Johnson, B. J., Sterling, C. W., Mohamad, M., Ogino, S. Y., Jordan, A., and da Silva, F. R.: First reprocessing of Southern Hemisphere ADditional OZonesondes (SHADOZ) profile records (1998-2015): 1. Methodology and evaluation, J. Geophys. Res., 122, 6611–6636, https://doi.org/10.1002/2016JD026403, 2017.

Yang, Y., Zhou, M., Langerock, B., Sha, M. K., Hermans, C., Wang, T., Ji, D., Vigouroux, C., Kumps, N., Wang, G., De Mazière, M., , and Wang, P.: A new site: ground-based FTIR XCO2, XCH4 and XCO measurements at Xianghe, China, Earth Syst. Sci. Data Discuss., https://doi.org/10.5194/essd-2019-172, in review, 2019.

Zhang, H., Xie, B., Zhao, S.-Y., and Chen, Q.: PM2.5 and tropospheric O3 in China and an analysis of the impact of pollutant emission control, Adv. Clim. Chang. Res., 5, 136–141, https://doi.org/10.1016/J.ACCRE.2014.11.005, 2014a.

Zhang, J., Xuan, Y., Yan, X., Liu, M., Tian, H., Xia, X., Pang, L., and Zheng, X.: Development and preliminary evaluation of a double-cell ozonesonde, Adv. Atmos. Sci., 31, 938–947, https://doi.org/10.1007/s00376-013-3104-1, 2014b.

Zheng, X., Xuan, Y., Lin, W., Tang, J., Tian, H., Zhang, J., and Xing, Y.: Performance Tests and Outdoor Comparison Observations of Domestic Remade ECC Ozonesondes, J. Appl. Meteorol. Sci., 29, 460–473, https://doi.org/10.11898/1001-7313.20180407, 2018.

Zhou, M., Vigouroux, C., Langerock, B., Wang, P., Dutton, G., Hermans, C., Kumps, N., Metzger, J.-M., Toon, G., and De Mazière, M.: CFC-11, CFC-12 and HCFC-22 ground-based remote sensing FTIR measurements at Réunion Island and comparisons with MIPAS/ENVISAT data, Atmos. Meas. Tech., 9, 5621–5636, https://doi.org/10.5194/amt-9-5621-2016, 2016.

Zhou, M., Langerock, B., Vigouroux, C., Sha, M. K., Ramonet, M., Delmotte, M., Mahieu, E., Bader, W., Hermans, C., Kumps, N., Metzger, J.-M., Duflot, V., Wang, Z., Palm, M., and De Mazière, M.: Atmospheric CO and CH4 time series and seasonal variations on Reunion Island from ground-based in-situ and FTIR (NDACC and TCCON) measurements, Atmos. Chem. Phys., 18, 13 881–13 901, https://doi.org/10.5194/acp-18-13881-2018, 2018.